

Effect of nonlinear magnon interactions on the stochastic magnetization switching

Mehrdad Elyasi,^{1,2} Shun Kanai,^{3,4,1,2,5,6,7} Hideo Ohno,^{2,8}
Shunsuke Fukami,^{3,4,1,2,8,9} and Gerrit E. W. Bauer^{1,2,10,11}

¹*Advanced Institute for Materials Research, Tohoku University, Sendai 980-8577, Japan*

²*Center for Science and Innovation in Spintronics,
Tohoku University, 2-1-1 Katahira, Sendai 980-8577, Japan.*

³*Laboratory for Nanoelectronics and Spintronics, Research Institute of Electrical Communication,
Tohoku University, 2-1-1 Katahira, Sendai 980-8577, Japan*

⁴*Graduate School of Engineering, Tohoku University,
6-6 Aramaki Aza Aoba, Sendai 980-8579, Japan.*

⁵*PRESTO, Japan Science and Technology Agency (JST), Kawaguchi 332-0012, Japan.*

⁶*Division for the Establishment of Frontier Sciences of Organization for Advanced
Studies at Tohoku University, Tohoku University, Sendai 980-8577, Japan.*

⁷*National Institutes for Quantum Science and Technology.*

⁸*Center for Innovative Integrated Electronic Systems,
Tohoku University, 468-1 Aramaki Aza Aoba, Sendai 980-8572, Japan.*

⁹*Inamori Research Institute of Science, Shijo, Shimogyo-ku, Kyoto 600-8411, Japan.*

¹⁰*Kavli Institute for Theoretical Sciences, University of the Chinese Academy of Sciences, Beijing 10090, China*

¹¹*Zernike Institute for Advanced Materials, University of Groningen, 9747 AG Groningen, Netherlands*

Telegraph noise caused by frequent switching of the magnetization in small magnetic devices has become a useful resource for probabilistic computing. Conventional theories have been based on a linearization of the fluctuations at the extrema of the magnetic free energy. We show theoretically that the non-linearities, specifically four-magnon scatterings, reduce the equilibrium fluctuation amplitude of the magnetization as well as the switching frequencies between local minima via the decay of the homogeneous Kittel mode into two spin waves with opposite momenta. Selectively suppressing the effective temperature of the finite- k spin waves, or reducing the radius of a thin magnetic disk enhance the switching frequency and improve performance of magnetic tunnel junctions in probabilistic computing applications.

I. INTRODUCTION

Fluctuations in magnetic materials are unwanted in applications such as data storage and communication, but are also essential for probabilistic computing or quantum information with magnetic devices. Research on magnetic noise focuses on either (i) the large fluctuations associated with equilibrium random telegraph noise (RTN)[1–5] and quantum tunneling of the magnetization [6, 7], as well as the Barkhausen noise due to moving magnetic textures [8, 9], or (ii) the small fluctuations around the equilibrium magnetization, e.g. thermal noise of spin waves including the uniform (Kittel) mode [10–16]. Under nonlinear (parametric) excitation, multi-stability of the magnetization can be established in the dynamical phase space that allows to manipulate the RTN and quantum tunneling between attractors [17, 18]. On the other hand, the magnetization in a magnet is generally bistable, which becomes a source of RTN [3, 4, 19, 20] and can be a resource in probabilistic computing [21–27]. While advances in fabricating dedicated magnetic tunnel junctions (MTJ) [28–30] already led to prototype devices [4, 22, 26, 27, 31] that could solve specific problems such as combinatorial optimization, the computing speed is still an issue.

Néel and Brown [1–3] formulated the RTN in a ferromagnetic particle based on Kramers escape theory [32] applied to the macrospin. In sufficiently large particles,

thermally activated magnetization reversal may also occur through domain wall nucleation and motion [33–39]. Braun’s [33–36] theory and that of others [38] linearize the fluctuations around stable points of the dynamics and therefore do not capture magnon interactions that emerge from the nonlinearities at large fluctuations.

Phenomenologically, RTN is characterized by a stochastic switching frequency f_s that must be high for probabilistic computing applications [4, 5, 40]. The Arrhenius law $f_s = f_0 e^{-E_B/k_B T}$ holds for any thermally activated reaction [41], where f_0 is the attempt frequency, k_B is the Boltzmann constant, E_B is a barrier energy, and T is the temperature. We recently found experimentally that the attempt time $\tau_0 = 1/f_0$ in magnetic tunnel junctions is larger than expected for a macrospin model [42, 43]. Nonuniform switching via domain walls would explain an increase rather than a decrease of f_s [33, 35, 37, 38] and therefore cannot explain the observations. Here, we demonstrate that the decay of the Kittel macrospin into spin waves with finite linear momentum can explain the observed brake on the stochastic switching.

In Sec. II, we show how magnon interactions affect the equilibrium amplitude distribution of the spatially uniform magnon (Kittel mode). In Sec. II A, we introduce the master equation for the Kittel magnon mode coupled to a pair of spin waves. In Sec. II B, we analyze the effects of magnon interactions on the distribution function and the effective magnon occupation numbers. In

Sec. II C, we show numerical results for the equilibrium magnon numbers and distribution functions. In Sec. III, we focus on the effect of nonlinear magnon interactions on the RTN. In Sec. III A, we briefly review different approaches to calculate f_s , viz. exact calculations for the macrospin model and theories based on linearization around the free energy extrema in the presence of domain walls. In Sec. III B, we introduce a simplified model for an easy numerical analysis of the macrospin RTN including magnon interactions. In Sec. III C, we discuss a phenomenological analysis and the full numerical model for the effect of nonlinear interactions on the RTN.

II. EQUILIBRIUM DISTRIBUTION OF INTERACTING MAGNONS

The thermal switching without external drive corresponds to rare large fluctuations in the equilibrium. According to the fluctuation dissipation theorem these can be expressed in terms of the linear response to a temperature or magnon density difference between different modes that induce spin and heat currents between them. We first focus on the equilibrium fluctuations of the Kittel and finite- k spin wave modes around a stable magnetization direction that form the input for Kramers's and Langer's theories for the switching frequency f_s in Sec. III. The free layer of state-of-the-art MTJs contain a disk of ultrathin magnetic films with thickness of a few nanometer and lateral dimensions of a few tens of nanometer. The exchange interaction then dominates the dispersion and shifts the nonuniform modes to energies above the ferromagnetic resonance of the lowest (homogeneous) Kittel mode.

According to the fluctuation dissipation theorem, we may approach the stochastics of a strictly equilibrium system in terms of the response to a thermodynamic force such as a temperature gradient. The latter can also be intentionally studied for example by mode-selective active cooling [44]. The latter selectivity would be easier to achieve for small magnets because the magnon spectrum is discrete and finite- k magnons are far detuned from the Kittel mode. In the following we therefore consider reservoirs of different magnon modes that may be at different temperatures.

A. Model

The magnon Hamiltonian of the Kittel mode and spin waves up to the fourth order in the Holstein-Primakoff

expansion reads [11, 18, 45, 48]

$$\mathcal{H} = \sum_{\vec{k}} \omega_{\vec{k}} c_{\vec{k}}^{\dagger} c_{\vec{k}} + \mathcal{H}^{(Suhl)} + \mathcal{H}^{(SK)} + \mathcal{H}^{(CK)}, \quad (1)$$

$$\mathcal{H}^{(Suhl)} = \sum_{\vec{k}, \vec{k}_1, \vec{k}_2} \mathcal{D}_{\vec{k}, \vec{k}_1, \vec{k}_2, \vec{k} + \vec{k}_1 - \vec{k}_2} c_{\vec{k}}^{\dagger} c_{\vec{k}_1}^{\dagger} c_{\vec{k}_2} c_{\vec{k} + \vec{k}_1 - \vec{k}_2} + H.c., \quad (2)$$

$$\mathcal{H}^{(SK)} = \sum_{\vec{k}} \mathcal{D}_{\vec{k}, \vec{k}, \vec{k}, \vec{k}} c_{\vec{k}}^{\dagger} c_{\vec{k}}^{\dagger} c_{\vec{k}} c_{\vec{k}}, \quad (3)$$

$$\mathcal{H}^{(CK)} = \sum_{\vec{k}, \vec{k}_1} \mathcal{D}_{\vec{k}, \vec{k}_1, \vec{k}, \vec{k}_1} c_{\vec{k}}^{\dagger} c_{\vec{k}}^{\dagger} c_{\vec{k}_1} c_{\vec{k}_1} (1 - \delta_{\vec{k}, \vec{k}_1}), \quad (4)$$

where $\mathcal{D}_{\vec{k}, \vec{k}_1, \vec{k}_2, \vec{k}_3}$ are the strengths of the interaction $c_{\vec{k}}^{\dagger} c_{\vec{k}_1}^{\dagger} c_{\vec{k}_2} c_{\vec{k}_3}$ that depend on material parameters, sample geometry, and magnetic field strength and direction. We assume that the magnet is so thin that three magnon scattering is not resonant, i.e. the Kittel mode frequency $\omega_0 < \omega_{\vec{k} \neq 0}$, and only renormalizes the four magnon scattering amplitudes [45].

The master equation governing the density matrix equation of motion (EOM) [46, 47],

$$\dot{\rho} = -i[\mathcal{H}, \rho] + \sum_{\vec{k}} \xi_{\vec{k}} L_{\vec{k}}^{(L)}[\rho],$$

where $\xi_{\vec{k}} = \alpha_G \omega_{\vec{k}}$ is the dissipation rate of the magnon mode with wave vector \vec{k} , α_G is the Gilbert damping assumed to be the same for all wave vectors, while the Lindblad dissipation operator

$$L_{\vec{k}}^{(L)} = (\bar{n}_{\vec{k}} + 1)(2c_{\vec{k}} \rho c_{\vec{k}}^{\dagger} - c_{\vec{k}}^{\dagger} c_{\vec{k}} \rho - \rho c_{\vec{k}}^{\dagger} c_{\vec{k}}) + \bar{n}_{\vec{k}}(2c_{\vec{k}}^{\dagger} \rho c_{\vec{k}} - c_{\vec{k}}^{\dagger} c_{\vec{k}} \rho - \rho c_{\vec{k}}^{\dagger} c_{\vec{k}}), \quad (5)$$

with $\bar{n}_{\vec{k}} = [\exp(\hbar\omega_{\vec{k}}/k_B T_{\vec{k}}) - 1]^{-1}$, is the average number of thermal bosons thermalized by baths at possibly different equilibrium temperatures $T_{\vec{k}}$. The different bath temperatures model selectively heated or cooled magnon modes, that bring the system into a non-equilibrium state.

For simplicity, we focus on a limited Hilbert space consisting of the Kittel mode and a pair of magnons with opposite momenta $\pm \vec{k}_{NU}$ and smallest detuning from the Kittel mode [see Fig. 1(a)], which is motivated by the strong decay of nonlinear effects as a function of energy differences. This model becomes better in the limit of small magnets with a discrete spectrum. The single pair approximation is justified for the IP case in which dipolar interaction create minima in the magnon frequency dispersion parallel to the magnetization with the largest $|\mathcal{D}^{(Suhl)}|$. The dispersion in the OOP is non-monotonic and isotropic, i.e. there is no clearly dominant pair. However, the nonlinear interactions on the Kittel mode dynamics remains the same. Since more than one pair will contribute to the dynamics,

our calculations of the RTN provide a lower bound estimate in this case. We specify \vec{k}_{NU} and associated model parameters for relevant magnetization configurations in magnetic tunnel junctions in Section III. The reduced Hamiltonian \mathcal{H}' contains the Suhl interaction $\mathcal{H}'^{(\text{Suhl})} = \mathcal{D}^{(\text{Suhl})} c_0^\dagger c_0^\dagger c_{\vec{k}_{NU}}^\dagger c_{-\vec{k}_{NU}} + \text{H.c.}$, the cross-Kerr interaction as $\mathcal{H}'^{(\text{CK})} = \mathcal{D}^{(\text{CK})} c_0^\dagger c_0^\dagger (c_{\vec{k}_{NU}}^\dagger c_{\vec{k}_{NU}} + c_{-\vec{k}_{NU}}^\dagger c_{-\vec{k}_{NU}})$, and self-Kerr interaction as $\mathcal{H}'^{(\text{SK})} = \sum_{\vec{k} \in \{0, \pm \vec{k}_{NU}\}} \mathcal{D}_{\vec{k}}^{(\text{SK})} c_{\vec{k}}^\dagger c_{\vec{k}}^\dagger c_{\vec{k}} c_{\vec{k}}$. We refer to $(c_0^\dagger c_0^\dagger c_{\vec{k}_{NU}}^\dagger c_{-\vec{k}_{NU}} + \text{H.c.})$ as ‘Suhl’ interaction, because it causes the second order Suhl instability of the Kittel mode [11, 18, 48–53]. The associated density matrix is ρ' .

B. Analytical analysis

A convenient measure of the density matrix ρ' is the Wigner distribution function

$$W'(\alpha_0, \alpha_{\vec{k}_{NU}}, \alpha_{-\vec{k}_{NU}}) = \frac{1}{\pi^2} \int d^2\mathfrak{z}_0 \int d^2\mathfrak{z}_{\vec{k}_{NU}} \int d^2\mathfrak{z}_{-\vec{k}_{NU}} \text{Tr} \left(\rho' \prod_{\vec{k} \in \{0, \pm \vec{k}_{NU}\}} e^{i\mathfrak{z}_{\vec{k}}^* c_{\vec{k}}^\dagger} e^{i\mathfrak{z}_{\vec{k}} c_{\vec{k}}} \right) \prod_{\vec{k} \in \{0, \pm \vec{k}_{NU}\}} e^{-i\mathfrak{z}_{\vec{k}}^* \alpha_{\vec{k}}^*} e^{-i\mathfrak{z}_{\vec{k}} \alpha_{\vec{k}}}, \quad (6)$$

where $\mathfrak{z}_{\vec{k}}$ is a complex variable, and $\alpha_{\vec{k}}$ is the stochastic complex variable corresponding to $c_{\vec{k}}$. $\text{Re}[\alpha_{\vec{k}}]$ ($\text{Im}[\alpha_{\vec{k}}]$) corresponds to the y' (z') components of the dynamic magnetization of mode \vec{k} , when the equilibrium magnetization is along \hat{x}' . The equation of motion of W' can be derived from the master equation using standard approaches [46, 54]. In Ref. [18], we obtained the following

Fokker-Planck-like equation (FPE) of motion

$$\begin{aligned} \frac{\partial W'}{\partial t} &= [W'_L + W'_D + W'_{\text{Suhl}} + W'_{\text{SK}} + W'_{\text{CK}}] W', \quad (7) \\ W'_L &= \sum_{\vec{k} \in \{0, \pm \vec{k}_{NU}\}} \left[i\omega_{\vec{k}} \frac{\partial}{\partial \alpha_{\vec{k}}} \alpha_{\vec{k}} + \text{c.c.} \right], \quad (8) \\ W'_D &= \sum_{\vec{k} \in \{0, \pm \vec{k}_{NU}\}} \left[\xi_{\vec{k}} \frac{\partial}{\partial \alpha_{\vec{k}}} \alpha_{\vec{k}} + \xi_{\vec{k}} (\bar{n}_{\vec{k}} + \frac{1}{2}) \frac{\partial^2}{\partial \alpha_{\vec{k}} \alpha_{\vec{k}}^*} + \text{c.c.} \right], \quad (9) \\ W'_{\text{Suhl}} &= i\mathcal{D}^{(\text{Suhl})} \left[2 \frac{\partial}{\partial \alpha_0} \alpha_0^* \alpha_{-\vec{k}} - \frac{\partial}{\partial \alpha_{-\vec{k}_{NU}}^*} \alpha_0^{*2} \alpha_{-\vec{k}} - \frac{\partial}{\partial \alpha_{\vec{k}_{NU}}^*} \alpha_0^{*2} \alpha_{-\vec{k}} - \frac{1}{4} \frac{\partial^3}{\partial \alpha_0^2 \partial \alpha_{-\vec{k}_{NU}}^*} \alpha_{\vec{k}_{NU}} - \frac{1}{4} \frac{\partial^3}{\partial \alpha_0^2 \partial \alpha_{\vec{k}_{NU}}^*} \alpha_{-\vec{k}_{NU}} + \frac{1}{2} \frac{\partial^3}{\partial \alpha_0 \partial \alpha_{\vec{k}_{NU}}^* \partial \alpha_{-\vec{k}_{NU}}^*} \alpha_0^* \right] + \text{c.c.}, \quad (10) \end{aligned}$$

$$\begin{aligned} W'_{\text{SK}} &= \sum_{\vec{k} \in \{0, \pm \vec{k}_{NU}\}} i\mathcal{D}_{\vec{k}}^{(\text{SK})} \left[2 \frac{\partial}{\partial \alpha_{\vec{k}}} |\alpha_{\vec{k}}|^2 \alpha_{\vec{k}} + \frac{1}{2} \frac{\partial^3}{\partial \alpha_{\vec{k}} \partial \alpha_{\vec{k}}^* \partial \alpha_{\vec{k}}^*} \alpha_{\vec{k}}^* \right] + \text{c.c.}, \quad (11) \end{aligned}$$

$$\begin{aligned} W'_{\text{CK}} &= \sum_{\vec{k} \in \{\pm \vec{k}_{NU}\}} i\mathcal{D}^{(\text{CK})} \left[\frac{\partial}{\partial \alpha_0} |\alpha_{\vec{k}}|^2 \alpha_0 + \frac{\partial}{\partial \alpha_{\vec{k}}} |\alpha_0|^2 \alpha_{\vec{k}} + \frac{1}{4} \frac{\partial^2}{\partial \alpha_0 \alpha_0^*} \alpha_{\vec{k}}^* + \frac{1}{4} \frac{\partial^2}{\partial \alpha_{\vec{k}} \alpha_{\vec{k}}^*} \alpha_0^* \right] + \text{c.c.}, \quad (12) \end{aligned}$$

that follows from the master equation for ρ' .

In the absence of non-linearities $\mathcal{D}^{(\text{Suhl})} = \mathcal{D}_{\vec{k}}^{(\text{SK})} = \mathcal{D}^{(\text{CK})} = 0$, the steady state solution of the FPE, Eq. (7), becomes

$$W'_{\text{ss}} = \mathcal{N} \exp \left(-\frac{2|\alpha_0|^2}{\bar{n}_0} - \frac{2|\alpha_{\vec{k}_{NU}}|^2}{\bar{n}_{\vec{k}_{NU}}} - \frac{2|\alpha_{-\vec{k}_{NU}}|^2}{\bar{n}_{-\vec{k}_{NU}}} \right), \quad (13)$$

where \mathcal{N} is a normalization constant. When $\mathcal{D}^{(\text{Suhl})} = 0$, but $\mathcal{D}_{\vec{k}}^{(\text{SK})} \neq 0$ or $\mathcal{D}^{(\text{CK})} \neq 0$, $W'_{\text{SK}} W'_{\text{ss}} = W'_{\text{CK}} W'_{\text{ss}} = 0$, i.e., W'_{ss} is still the steady state solution. When $\mathcal{D}^{(\text{Suhl})} \neq 0$,

$$\begin{aligned} W'_{\text{Suhl}} W'_{\text{ss}} &= i\mathcal{D}^{(\text{Suhl})} \left(-\frac{4}{\bar{n}_0} + \frac{4}{\bar{n}_{\pm \vec{k}_{NU}}} + \frac{4}{\bar{n}_{\pm \vec{k}_{NU}} \bar{n}_0^2} - \frac{4}{\bar{n}_{\pm \vec{k}_{NU}}^2 \bar{n}_0} \right) + \text{c.c.} \quad (14) \end{aligned}$$

According to equation (14) and $\bar{n}_0 = \bar{n}_{\pm \vec{k}_{NU}}$, $W'_{\text{Suhl}} W'_{\text{ss}} = 0$, and W'_{ss} still holds for the steady state. However, when $\bar{n}_0 \neq \bar{n}_{\pm \vec{k}_{NU}}$, $W'_{\text{Suhl}} W'_{\text{ss}} \neq 0$, and W'_{ss} does not solve the problem anymore.

Since finding the steady state solution W' when $\mathcal{D}^{(\text{Suhl})} \neq 0$ is a formidable task, we focus on the magnon numbers $\langle n_{\vec{k}} \rangle = \langle c_{\vec{k}}^\dagger c_{\vec{k}} \rangle$. The master equation for ρ' reduces then to

$$\frac{d\mathcal{X}}{dt} = i2\Delta\omega_{\pm\vec{k}_{NU}}\mathcal{X} - i\mathcal{D}^{(\text{Suhl})} \left[(4\langle n_0 \rangle + 2)\langle n_{\vec{k}_{NU}} \rangle^2 - (4\langle n_{\vec{k}_{NU}} \rangle + 2)\langle n_0 \rangle^2 \right] - 2(\xi_0 + \xi_{\pm\vec{k}_{NU}})\mathcal{X}, \quad (15)$$

$$\frac{d\langle n_0 \rangle}{dt} = -2\mathcal{D}^{(\text{Suhl})}\text{Im}[\mathcal{X}] - 2\xi_0(\langle n_0 \rangle - \bar{n}_0), \quad (16)$$

$$\frac{d\langle n_{\pm\vec{k}_{NU}} \rangle}{dt} = 2\mathcal{D}^{(\text{Suhl})}\text{Im}[\mathcal{X}] - 2\xi_{\pm\vec{k}_{NU}}(\langle n_{\pm\vec{k}_{NU}} \rangle - \bar{n}_{\pm\vec{k}_{NU}}), \quad (17)$$

where $\mathcal{X} = \langle c_0 c_0 c_{\vec{k}_{NU}}^\dagger c_{-\vec{k}_{NU}}^\dagger \rangle$.

An analytical solution for the steady state of the EOMs Eqs. (15)-(17) can be found for small deviations x in $\langle n_0 \rangle = \bar{n}_0 + x$ and y in $\langle n_{\pm\vec{k}_{NU}} \rangle = \bar{n}_{\pm\vec{k}_{NU}} + y$. To leading order

$$x = \frac{\mathcal{D}^{(\text{Suhl})2}(\xi_0 + \xi_{\pm\vec{k}_{NU}})}{(\xi_0 + \xi_{\pm\vec{k}_{NU}})^2 + \Delta\omega_{\pm\vec{k}_{NU}}^2} \frac{f(\bar{n}_0, \bar{n}_{\pm\vec{k}_{NU}})}{g(\bar{n}_0, \bar{n}_{\pm\vec{k}_{NU}})}$$

$$y = \frac{-\xi_0}{\xi_{\pm\vec{k}_{NU}}}x, \quad (18)$$

where

$$f(\bar{n}_0, \bar{n}_{\pm\vec{k}_{NU}}) = 2(\bar{n}_{\pm\vec{k}_{NU}}^2 - \bar{n}_0^2) + 4(\bar{n}_0\bar{n}_{\pm\vec{k}_{NU}}^2 - \bar{n}_0^2\bar{n}_{\pm\vec{k}_{NU}})$$

$$g(\bar{n}_0, \bar{n}_{\pm\vec{k}_{NU}}) = 2\xi_0 + \frac{(\mathcal{D}^{(\text{Suhl})})^2(\xi_0 + \xi_{\pm\vec{k}_{NU}})}{(\xi_0 + \xi_{\pm\vec{k}_{NU}})^2 + \Delta\omega_{\pm\vec{k}_{NU}}^2} \times$$

$$\left[\left(4\bar{n}_{\pm\vec{k}_{NU}}^2 - 8\bar{n}_0\bar{n}_{\pm\vec{k}_{NU}} - 4\bar{n}_0 \right) + \frac{\xi_0}{\xi_{\pm\vec{k}_{NU}}} \times \left(4\bar{n}_0^2 - 8\bar{n}_0\bar{n}_{\pm\vec{k}_{NU}} - 4\bar{n}_{\pm\vec{k}_{NU}} \right) \right]. \quad (19)$$

When $\bar{n}_0 = \bar{n}_{\pm\vec{k}_{NU}} = 0$, $f(\bar{n}_0, \bar{n}_{\pm\vec{k}_{NU}}) = 0$, thus $x = y = 0$ as expected. When $\bar{n}_0 > \bar{n}_{\pm\vec{k}_{NU}}$ ($\bar{n}_0 < \bar{n}_{\pm\vec{k}_{NU}}$), $x < 0$ ($x > 0$) and $y > 0$ ($y < 0$), i.e., the Kittel and the $\pm\vec{k}_{NU}$ magnons equilibrate towards temperatures that are governed by the reservoirs.

C. Numerical results and discussion

In the steady state, Eqs. (15)-(17) reduce to a polynomial equation in $\langle n_{\pm\vec{k}_{NU}} \rangle$ and $\langle n_0 \rangle$. Figure 1(a) shows the dependence of $\langle n_0 \rangle - \bar{n}_0$ for fixed \bar{n}_0 as a function of $\bar{n}_{\pm\vec{k}_{NU}}$ and $\mathcal{D}^{(\text{Suhl})}$ ($\mathcal{D}^{(\text{SK})} = \mathcal{D}^{(\text{CK})} = 0$). When $\bar{n}_0 > \bar{n}_{\pm\vec{k}_{NU}}$ ($\bar{n}_0 < \bar{n}_{\pm\vec{k}_{NU}}$) we find that $\langle n_0 \rangle < \bar{n}_0$ ($\langle n_0 \rangle > \bar{n}_0$), as expected from the analysis in Sec. II B and Eqs. (18)-(19). For fixed $\bar{n}_{\pm\vec{k}_{NU}}$, $|\langle n_0 \rangle - \bar{n}_0|$ increases and eventually saturates with increasing $|\mathcal{D}^{(\text{Suhl})}|$,

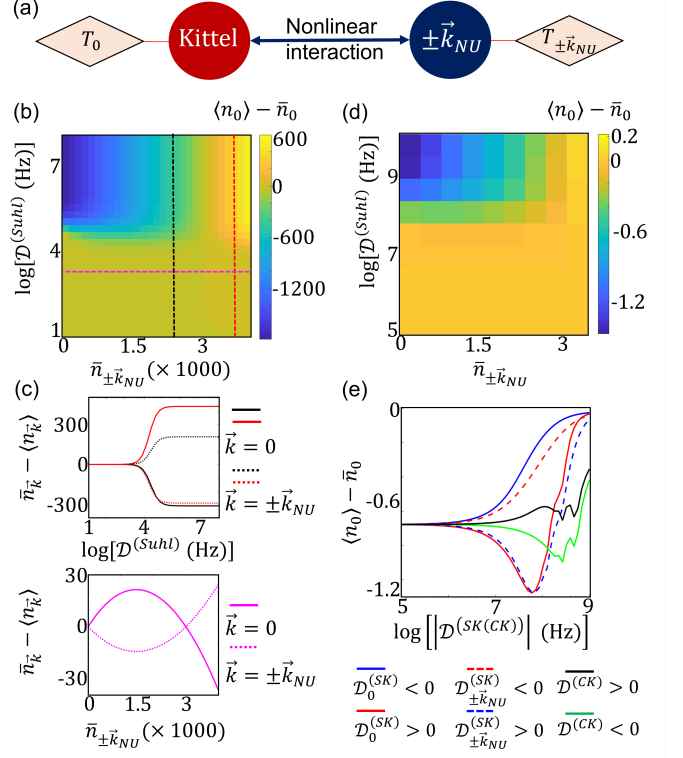


FIG. 1. Occupation numbers in the interacting model of Fig. 1(a). (a) A schematic of the Kittel and $\pm\vec{k}_{NU}$ modes coupled to separate thermal baths. (b) $\langle n_0 \rangle - \bar{n}_0$ as a function of $\bar{n}_{\pm\vec{k}_{NU}}$ and $|\mathcal{D}^{(\text{Suhl})}|$, as calculated from Eqs. (15)-(17) for $\bar{n}_0 = 3000$. (c) Dependence of $\bar{n}_{\vec{k}} - \langle n_{\vec{k}} \rangle$ on selected values of $\mathcal{D}^{(\text{Suhl})}$ (top) and $\bar{n}_{\pm\vec{k}_{NU}}$ (bottom). The black (red) lines correspond to $\bar{n}_{\pm\vec{k}_{NU}}$ as indicated in (a). The magenta lines correspond to $\mathcal{D}^{(\text{Suhl})}$ as indicated in (a). (d) Same as (a) but calculated from numerical solutions of ρ' for $\bar{n}_0 = 3$. In (b)-(d), $\mathcal{D}^{(\text{SK})} = \mathcal{D}^{(\text{CK})} = 0$. (e) $\langle n_0 \rangle - \bar{n}_0$ as a function of $\mathcal{D}_0^{(\text{SK})}$, $\mathcal{D}_{\pm\vec{k}_{NU}}^{(\text{SK})}$, and $\mathcal{D}^{(\text{CK})}$, while $\mathcal{D}^{(\text{Suhl})} = 0.1$ GHz, $\bar{n}_0 = 3$, and $\bar{n}_{\pm\vec{k}_{NU}} = 1.5$. In (b)-(e) $\xi_0/(2\pi) = \xi_{\pm\vec{k}_{NU}}/[2\pi \times (1 + \alpha_G \Delta\omega_{\pm\vec{k}_{NU}}/\omega_0)] = 1.5$ MHz, $\Delta\omega_{\pm\vec{k}_{NU}}/(2\pi) = 0.5$ GHz.

approaching complete equilibration between the Kittel mode and the magnon pair to a common temperature. Figure 1(c) shows examples of $\bar{n}_{\vec{k}} - \langle n_{\vec{k}} \rangle$ for both $\vec{k} = 0$ and $\vec{k} = \pm\vec{k}_{NU}$ as functions of $\mathcal{D}^{(\text{Suhl})}$ and $\bar{n}_{\pm\vec{k}_{NU}}$, at $\bar{n}_{\pm\vec{k}_{NU}}$ and $\mathcal{D}^{(\text{Suhl})}$ values as indicated by the straight lines of the same color in Fig. 1(b).

We must keep in mind that approximations are valid only for temperatures that correspond to small \bar{n}_0 and $\bar{n}_{\pm\vec{k}_{NU}}$. Figure 1(c) and Fig. 1(a) are similar (except for $\bar{n}_0 = 3$), as expected. Figure 1(e) shows $\langle n_0 \rangle - \bar{n}_0$ as a function of $\mathcal{D}_0^{(\text{SK})}$, $\mathcal{D}_{\pm\vec{k}_{NU}}^{(\text{SK})}$, and $\mathcal{D}^{(\text{CK})}$ for a fixed $\mathcal{D}^{(\text{Suhl})} \neq 0$, and $\bar{n}_0 \neq \bar{n}_{\pm\vec{k}_{NU}}$. The self-Kerr and cross-Kerr interactions lead to the frequency shifts $\Delta\omega_{\pm\vec{k}_{NU}}$. An increase (decrease) in $\Delta\omega_{\pm\vec{k}_{NU}}$ naturally decreases (in-

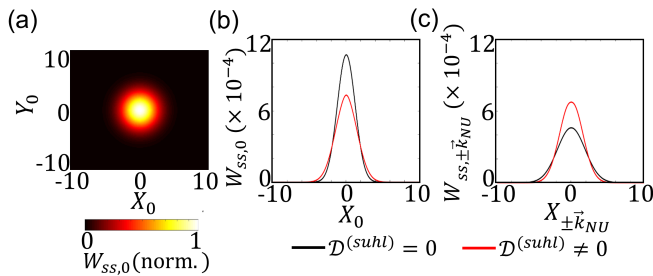


FIG. 2. Wigner function of three-level magnon system. (a) $W'_{ss,0}(X_0, Y_0)$, when $\bar{n}_0 = 0$, and $\mathcal{D}^{(\text{Suhl})} = 0$. (b) and (c) $W'_{ss,0}$ and $W'_{\pm\vec{k}_{NU}}$, respectively, for $\mathcal{D}^{(\text{Suhl})} = 0$ and $\mathcal{D}^{(\text{Suhl})} = 0.1$ GHz, $\bar{n}_0 = 3$, $\bar{n}_{\pm\vec{k}_{NU}} = 1.5$, $\mathcal{D}^{(\text{Suhl})} = 0.1$ GHz, and $\mathcal{D}^{(SK)} = \mathcal{D}^{(CK)} = 0$. The other parameters are those used in Fig. 1.

creases) $|\langle n_0 \rangle - \bar{n}_0|$ [see Eq. (18)].

Figure 2(a) shows the equilibrium Wigner function of the Kittel mode, $W'_{ss,0}(X_0, Y_0)$ for $\mathcal{D}^{(\text{Suhl})} = 0$, where $W'_{ss,\vec{k}}(X_{\vec{k}}, Y_{\vec{k}})$ is the steady state Wigner function of \vec{k} mode after tracing out the other modes, $X_{\vec{k}} = \text{Re}[\alpha_{\vec{k}}]$ and $Y_{\vec{k}} = \text{Im}[\alpha_{\vec{k}}]$. The latter variables represent the dynamic magnetizations of modes with index \vec{k} by $\vec{M}_{\vec{k}} \cdot \hat{y}' = M_s X_{\vec{k}} / \sqrt{S}$ and $\vec{M}_{\vec{k}} \cdot \hat{z}' = M_s Y_{\vec{k}} / \sqrt{S}$ in a rotating frame, where S is the total spin and M_s is the saturation magnetization. Figures 2(b) and (c) show $W'_{ss,0}(X_0, 0)$ and $W'_{ss,\pm\vec{k}_{NU}}(X_{\pm\vec{k}_{NU}}, 0)$ (steady state Wigner function of either of the $\pm\vec{k}_{NU}$ modes), respectively, for $\mathcal{D}^{(\text{Suhl})} = 0$ (black lines) and $\mathcal{D}^{(\text{Suhl})} \neq 0$ (red lines). Since $\bar{n}_0 < \bar{n}_{\pm\vec{k}_{NU}}$, the magnon numbers equilibrate by shrinking (expanding) the Wigner function (relative to its form at $\mathcal{D}^{(\text{Suhl})} = 0$) of the \vec{k}_{NU} (Kittel) mode. In the following, we show how the distributions functions affect the RTN and switching frequency.

III. RANDOM TELEGRAPH NOISE BY MAGNETIZATION REVERSAL

A. Introduction

1. Magnetic tunnel junctions and magnon parametron

In Sec. II, we addressed the FPE-like EOM for the Wigner function [see Eq. (7)] of interacting magnons. Without a drive, the effective potential of each of the magnon modes has only one minimum. While not directly relevant for the present generation of experiments on MTJ, we point out here the relation with the “magnon parametron”, a magnetic disk that becomes bistable under a parametric excitation of the Kittel mode [17, 18]. Its two potential minima can be tuned into the stochastic switching regime [17, 18]. The distribution function $W_{\vec{m}}$

of the magnetization \vec{m} with constant modulus around each of the two minima is similar to the equilibrium $W'_{ss,0}$ (Wigner function of the Kittel mode steady state) derived above, but entails additional dynamical effects as demonstrated in this section. The FPE EOM for the distribution function $W_{\vec{m}}$ has the form

$$\frac{\partial W_{\vec{m}}}{\partial t} = \left[-\frac{\partial}{\partial x_i} \mathcal{A}_i(\vec{x}) + \frac{1}{2} \frac{\partial^2}{\partial x_i \partial x_j} \mathcal{B}_{ij}(\vec{x}) + \dots \right] W_{\vec{m}}, \quad (20)$$

where a summation over the repeated indices is implied, \mathcal{A}_i and \mathcal{B}_{ij} are model-dependent constants that govern the drift and diffusion terms, respectively, $\{i, j\} \in \{\theta, \phi\}$, and θ (ϕ) is the polar (azimuthal) angle of the magnetization. We can solve Eq. (20) by the ansatz

$$W_{\vec{m}} = W_{ss,\vec{m}} + \sum_n \mathcal{F}_n(\theta, \phi) e^{-a_n t}, \quad (21)$$

where $W_{ss,\vec{m}}$ is the steady state solution, while the a_n with the largest real part, a_1 , corresponds to the switching frequency [2, 18, 57], i.e., $f_s = a_1$. Solving $W_{\vec{m}}$ exactly is tedious and often impossible without additional approximations such as Kramers escape [32, 56] or high-barrier limit [55] assumptions, which we briefly review below.

2. Brown theory for the Kramers escape of macrospin

The Néel-Brown theory considers a macrospin with free energy $E(\theta, \phi)$, where θ is the angle with respect to the easy axis \hat{x} direction and ϕ is the azimuthal angle measured from the xy plane. The Kramers method is valid in the high energy barrier limit in the path of least action between the energy minima. Here, we briefly review the Brown theory for a ϕ -independent free energy $E = E(\theta)$, with two minima at $\theta_1 = 0$ and $\theta_2 = \pi$ and a saddle point (maximum in this 1D case) at $0 < \theta_{sd} < \pi$. The critical assumption is a Maxwell distribution for $[0, \theta_{r1}] \cup [\theta_{r2}, \pi]$, where $0 < \theta_{sd} < \theta_{r1} < \theta_{r2} < \theta_{sd} < \pi$, $W \approx W_{1(2)} = W_{1(2)}(0(\pi)) \exp\{-\beta[E_{1(2)}(\theta) - E(0(\pi))]\}$, $\beta = V_s/k_B T$, V_s is the sample volume, $E_{1(2)}(\theta) \approx E(0(\pi)) + E''(0(\pi))\theta^2$, and $E''(\theta) = (\partial^2 E / \partial \theta^2)|_{\theta}$. The total number of magnons close to the minima $[0, \theta_{r1}] \cup [\theta_{r2}, \pi]$ is $N_{1(2)} = \int_{0(\pi)}^{\theta_{r1}(\pi)} W_{1(2)} d\theta$. The integral can be carried out under the high barrier assumption or $\theta_{r1} \rightarrow \infty$ ($\theta_{r2} \rightarrow -\infty$) and $N_{1(2)} \approx W_{1(2)}(0(\pi)) \times [\beta E''(0(\pi))]^{-1}$.

The probability current \vec{J} through the saddle point is conserved and related to the distribution function by $\partial W / \partial t = -\nabla \cdot \vec{J}$ that in our case leads to $J_{\theta} = -\mathcal{A}_{\theta} W + \frac{1}{2} \mathcal{B}_{\theta,\theta} \partial W / \partial \theta$. Brown derived that $\mathcal{A}_{\theta} = -\mathbf{a} \partial E / \partial \theta$ and $\mathcal{B}_{\theta,\theta} = 2\mathbf{b} = \mathbf{a} / \beta$, and $\mathbf{a} = \alpha_G \times [\gamma^{-2} + (\alpha_G M_s)^2]^{-1}$, γ is the gyromagnetic constant and M_s is the saturation magnetization. After multiplying the latter with $\exp[\beta E(\theta)]$ and integrating over θ , $J_{\theta} = -\dot{N}_1 = \dot{N}_2 =$

$-v_{21}N_2 + v_{12}N_1$, where

$$v_{12}(v_{21}) = \mathbf{a}\sqrt{\beta\lambda_{sd}/(2\pi)}\lambda_{0(\pi)}\exp\{-\beta[E(\theta_{sd})-E(0(\pi))]\}, \quad (22)$$

and $\lambda_x = E''(x)$.

This approach can be extended to a ϕ -dependent system as long as it supports two (meta)stable states at θ_1 and θ_2 and a saddle node θ_{sd} that we assume to be at $\phi = 0$ without loss of generality, thereby reproducing [3]

$$v_{ij} = \mathcal{G} \frac{\alpha_G \gamma}{M_s(1 + \alpha_G^2)} \sqrt{\frac{-\lambda_{sd,\phi}}{\lambda_{sd,\theta}}} \sqrt{\lambda_{i,\phi}\lambda_{i,\theta}} e^{-\beta[E(\theta_{sd})-E(\theta_i)]}, \quad (23)$$

where $\mathcal{G} = (-2\lambda_{sd,\phi})^{-1} \times \{(-\lambda_{sd,\phi} - \lambda_{sd,\theta}) + [(-\lambda_{sd,\phi} - \lambda_{sd,\theta})^2 - 4\lambda_{sd,\phi}\lambda_{sd,\theta}/\alpha_G^2]^{1/2}\}$, $\lambda_{x,y} = (\partial^2 E/\partial y^2)|_{\theta_x}$. The switching frequency is therefore

$$f_s = a_1 = v_{12} + v_{21}. \quad (24)$$

3. Braun theory for nonuniform magnetization switching

The Néel-Brown theory relies on a magnetization that remains spatially uniform during the switching process. However, depending on the shape and size of the magnet, the applied magnetic field, and material parameters such as crystalline anisotropy and exchange length, the saddle point in the free energy may belong to a magnetic texture, even when the magnetization of the minima are uniform. For a wire with magnetic fields applied along the easy axis that are small compared with the anisotropy, Braun [33, 34] found saddle points of the free energy for two domain walls and derived an FPE starting from the linearized Landau-Lifshitz-Gilbert (LLG) with thermal fluctuations. The stochastic switching rate follows then from an extension of the Langer's theory for metastable decay [55] in the high barrier limit and assuming an equilibrium distributions $W_2 = 0$ around the stable state and $W_1 = W_{eqb} = Z^{-1}e^{-\beta E_{sd}^{(2)}}$ around the metastable one, where $E_{sd}^{(2)}$ is the expansion of free energy at the saddle point up to second order in θ (ϕ) of the fluctuations p (q). This approximation assumes that all magnons quasiparticles reside in the metastable region while none exist beyond the saddle point, i.e., $\int W_{eqb} dpdq = 1$ which fixes the partition function Z . The nonequilibrium distribution becomes $W = FW_{eqb}$, and F can be derived from the FPE, from which the probability current \vec{J} follows. The switching frequency is obtained by integration of \vec{J} over over all the dimensions transverse to the path of least action. For a cylindrical wire [34]

$$f_s = \mathcal{P} \sqrt{\frac{\det(\mathcal{H}_{m,q}) \det(\mathcal{H}_{m,p})}{\det'(|\mathcal{H}_{sd,q}|) \det(\mathcal{H}_{sd,p})}}, \quad (25)$$

where $\mathcal{H}_{sd(m),q(p)}$ are the second order expansion terms of the free energy in p and q close to the extrema, i.e. $E_{sd(m)}^{q(p)} = \int dx [p\mathcal{H}_{sd(m),p}p + q\mathcal{H}_{sd(m),q}q]$.

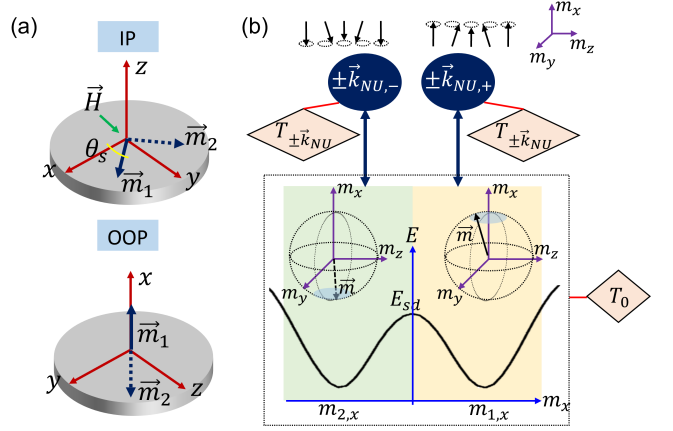


FIG. 3. Schematics of the two configurations of MTJs used to study stochastic switching. (a) Top panel: in-plane configuration, with easy axis anisotropy along \hat{x} , hard axis uniaxial anisotropy along \hat{z} , and a magnetic field applied along \hat{y} . Bottom panel: the out-of-plane (OOP) configuration, with easy axis uniaxial anisotropy along \hat{x} . In top and bottom panels, \vec{m}_1 and \vec{m}_2 are the equilibrium magnetization directions (minima of macrospin free energy). (b) A sketch of the model in Sec. III B emphasizing the difference of the three level systems in the two minima of the free energy.

$\det(\mathcal{H}_{sd(m),p(q)}) = \prod_{i \in \{bs, \vec{k}\}} \lambda_{sd(m),i}^{p(q)}$, where $\lambda_{sd(m),i}^{p(q)}$ are the eigenvalues of $\mathcal{H}_{sd(m),p(q)}$. 'bs' stands for bound states, and prime in \det' denotes exclusion of $\lambda_{sd(m),i} = 0$, i.e. the Goldstone modes corresponding to the translational invariance of the saddle node. $\mathcal{P} = \lambda_d \sqrt{E_{sd} - E_m} L \sqrt{\beta' \mathcal{S} / 2\pi^3}$, where \mathcal{S} (L) is the cross section (length) of the sample, $\beta' = 1/(k_B T)$, and only $\lambda_d > 0$ depends on the dynamics governed by the linearized LLG at the saddle node, viz. $\lambda_d \chi_{q,d} = -H_{sd,p} \chi_{p,d} - \alpha_G H_{sd,q} \chi_{q,d}$ and $\lambda_d \chi_{p,d} = H_{sd,q} \chi_{q,d} - \alpha_G H_{sd,p} \chi_{p,d}$, and $(\chi_{p,d}, \chi_{q,d})$ is the corresponding eigenfunction.

4. Magnon interactions

The theoretical approaches to compute f_s as summarized above linearize the free energy around the extrema. In Braun theory for nonuniform domain wall assisted magnetization switching, spin waves are assumed to be non-interacting. To the best of our knowledge, magnon interactions on the magnetization switching and RTN have generally been neglected. In Sec. III B, we introduce a minimal model for the effects of magnon interactions on the uniform magnetization dynamics. In Sec. III C 1, we discuss the phenomenology of nonlinear interactions in the RTN. In Sec. III C 2, we use the model from Sec. III B to numerically calculate and interpret the effect of four-magnon interactions on f_s . A full numerical solution of the LLG equation including thermal noise may be used to test our phenomenology.

B. Model

The stochastic switching of MTJs is explored for the in-plane (IP) and out-of-plane (OOP) configurations as sketched in Fig. 3(a) [4, 22, 40, 43]. We chose two coordinate systems such that the equilibrium magnetization without an applied field is always along the \hat{x} axis. In the IP configuration, the magnetization lies IP by a hard uniaxial anisotropy K_z along \hat{z} , while an elliptical shape defines an easy axis anisotropy K_x along \hat{x} . An IP applied magnetic field applied along \hat{y} then forces a finite angle θ_s between the equilibrium magnetization and \hat{x} [see Fig. 1(a)]. In the OOP configuration the magnetization is perpendicular to the plane, which in our definition defined the \hat{x} axis. This implies an easy axis uniaxial anisotropy K_x along \hat{x} . The free energy of the OOP macrospin is independent of azimuthal angle, while for the IP macrospin it depends on both the polar and azimuthal angles, which leads to different switching characteristics for the two configurations [2–4, 40]. Additionally, the magnon dispersion and the relevant interaction coefficients are different for the two. For example, for the IP case, the magnons with wavevector parallel to the magnetization have lower frequency than the perpendicular ones, while for the OOP case, the frequency of the magnons with in-plane wavevector does not depend on the in-plane angle. In Ref. [42], we already simulated the dynamics of the uniform magnetization (macrospin) coupled to a pair of spin waves with opposite in-plane wave vectors $\pm\vec{k}_{NU,i}$. Here $i \in \{+, -\}$ indicates the configuration space around the minima with $m_x > 0$ and $m_x < 0$, respectively. We pick a pair of magnons for each of the two energy wells as sketched in Fig. 3(b). The interaction with spin waves \vec{k}_{NU} generates an effective stochastic magnetic field $\vec{H}_{SW} = \vec{H}_{SW}^{(Suhl)} + \vec{H}_{SW}^{(CK)}$

on the macrospin by the 4-magnon interactions, where

$$\begin{aligned}
H_{SW,x}^{(Suhl)} &= \mathcal{C} \left\{ \text{Re} \left[\alpha_{\vec{k}'_{NU}} \alpha_{-\vec{k}'_{NU}} \right] \left\{ \mathcal{K} \sin \theta_s \times [m_x \sin \theta_s - \right. \right. \\
&\quad \left. \left. \text{sign}(m_x) m_y \cos \theta_s \right] + \mathcal{K}' \cos \theta_s \text{sign}(m_x) \right\} - \\
&\quad \left. \text{Im} \left[\alpha_{\vec{k}'_{NU}} \alpha_{-\vec{k}'_{NU}} \right] \sin \theta_s m_z \right\}, \\
H_{SW,y}^{(Suhl)} &= \mathcal{C} \left\{ \text{Re} \left[\alpha_{\vec{k}'_{NU}} \alpha_{-\vec{k}'_{NU}} \right] \left\{ \mathcal{K} \cos \theta_s \times [m_y \cos \theta_s - \right. \right. \\
&\quad \left. \left. |m_x| \sin \theta_s \right] + \mathcal{K}' \sin \theta_s \right\} + \text{Im} \left[\alpha_{\vec{k}'_{NU}} \alpha_{-\vec{k}'_{NU}} \right] \cos \theta_s m_z \right\}, \\
H_{SW,z}^{(Suhl)} &= \mathcal{C} \left\{ -\text{Im} \left[\alpha_{\vec{k}'_{NU}} \alpha_{-\vec{k}'_{NU}} \right] [m_x \sin \theta_s - \text{sign}(m_x) - \right. \\
&\quad \left. m_y \cos \theta_s \right] \mathcal{K} \times \text{Re} \left[\alpha_{\vec{k}'_{NU}} \alpha_{-\vec{k}'_{NU}} \right] m_z \right\}, \quad (26) \\
H_{SW,x}^{(CK)} &= \mathcal{C}' \left| \alpha_{\pm\vec{k}'_{NU}} \right|^2 \left\{ -\mathcal{K} \times \text{sign}(m_x) \cos \theta_s - 2\mathcal{K}'' \times \right. \\
&\quad \left. [2\sin^2 \theta_s m_x - 2\sin \theta_s \cos \theta_s \text{sign}(m_x) m_y] \right\}, \\
H_{SW,y}^{(CK)} &= \mathcal{C}' \left| \alpha_{\pm\vec{k}'_{NU}} \right|^2 \left\{ -\mathcal{K} \times \sin \theta_s - 2\mathcal{K}'' \times \right. \\
&\quad \left. [2\cos^2 \theta_s m_y - 2\sin \theta_s \cos \theta_s |m_x|] \right\}, \\
H_{SW,z}^{(CK)} &= \mathcal{C}' \left| \alpha_{\pm\vec{k}'_{NU}} \right|^2 \left\{ -2\mathcal{K}'' \times [-2m_z] \right\}, \quad (28)
\end{aligned}$$

and $\vec{H}_{SW}^{(Suhl)}$ and $\vec{H}_{SW}^{(CK)}$ derive from the Hamiltonians $\mathcal{H}^{(Suhl)}$ and $\mathcal{H}^{(CK)}$, respectively. Here $\mathcal{C} = -4\mathcal{D}_{\pm\vec{k}_{NU}}^{(Suhl)}/\gamma(1 + |m_x| \cos \theta_s + m_y \sin \theta_s)$, $\mathcal{K} = (u_0^2 + v_0^2)$, and $\mathcal{K}' = u_0 v_0 (1 + |m_x| \cos \theta_s + m_y \sin \theta_s)$. $\vec{k}'_{NU} = \vec{k}_{NU,+}$ ($\vec{k}'_{NU} = \vec{k}_{NU,-}$) when $m_x > 0$ ($m_x < 0$). $\mathcal{C}' = 2\mathcal{D}^{(CK)}/\gamma$ and $\mathcal{K}'' = u_0 v_0 / (1 + |m_x| \cos \theta_s + m_y \sin \theta_s)$. $u_0 = \sqrt{(A_0 + \omega_0)/(2\omega_0)}$, $v_0 = -\text{sign}(B_0) \sqrt{(A_0 - \omega_0)/(2\omega_0)}$, $A_0 = |\gamma\mu_0 H_y| + \omega_M (K_x \sin^2 \theta_s + K_z)/2$, $B_0 = \omega_M (K_x \sin^2 \theta_s - K_z)/2$, $\omega_0 = \sqrt{A_0^2 - |B_0|^2}$, and $\omega_M = \gamma M_s S = V_s M_s / (h\gamma)$ is the total number of spins in the magnet.

Vice versa, the dynamics of the macrospin parametrically excites the spin wave pairs via the Hamiltonian $\mathcal{H}^{(Suhl)} \equiv \sum_i P_i c_{\vec{k}_{NU,i}}^\dagger c_{-\vec{k}_{NU,i}}^\dagger + \text{H.c.}$, where

$$\begin{aligned}
P_i &= -\frac{S\gamma\mathcal{C}_i}{2} \left\{ \mathcal{K} \times \left[(|m_x| \sin \theta_s - m_y \cos \theta_s)^2 - m_z^2 \right] + \right. \\
&\quad \left. 2i [-m_x m_z \sin \theta_s + m_y m_z \text{sign}(m_x) \cos \theta_s] - \right. \\
&\quad \left. 2\mathcal{K}' [1 - |m_x| \cos \theta_s - m_y \sin \theta_s] \right\}, \quad (29)
\end{aligned}$$

$\mathcal{C}_{+(-)} = \mathcal{C}$ when $m_x > 0$ ($m_x < 0$) and zero otherwise. The cross-Kerr interaction $\mathcal{H}^{(CK)} \equiv \sum_{\vec{k} \in \{0, \pm\vec{k}_{NU, +(-)}\}} \omega'_k c_{\vec{k}}^\dagger c_{\vec{k}}$ leads to the dynamical frequency shift of the spin waves

$$\begin{aligned}
\Delta\omega'_{\pm\vec{k}_{NU,i}} &= \mathcal{D}_i^{(CK)} \times \left\{ SK (1 - \right. \\
&\quad \left. \cos \theta_s |m_x| - \sin \theta_s m_y) - 2S^2 \mathcal{K}' [\sin^2 \theta_s m_x^2 + \right. \\
&\quad \left. \cos^2 \theta_s m_y^2 - 2\sin \theta_s \cos \theta_s |m_x| m_y - m_z^2] \right\}, \quad (30)
\end{aligned}$$

where $\mathcal{D}_{+(-)}^{(CK)} = \mathcal{D}^{(CK)}$ when $m_x > 0$ ($m_x < 0$) otherwise zero. We can now formulate the coupled equations of motion that consist of the stochastic LLG equations for the Kittel mode

$$\begin{aligned} \frac{d\vec{m}}{dt} &= -\gamma\mu_0\vec{m} \times \left(\vec{H}_A + \vec{H}_{dc} + \vec{H}_{SW} + \vec{H}_{th} \right) + \quad (31) \\ \alpha_G\vec{m} \times \frac{d\vec{m}}{dt}, \end{aligned}$$

while following \dot{W}' (see Sec. II B), the spin wave pair obeys

$$\begin{aligned} \frac{dX_{\pm\vec{k}_{NU,i}}}{dt} &= -(\omega'_{\pm\vec{k}_{NU,i}} + \omega_{\pm\vec{k}_{NU,i}})Y_{\pm\vec{k}_{NU,i}} - \quad (32) \\ \alpha_G\omega_{\pm\vec{k}_{NU,i}}X_{\pm\vec{k}_{NU,i}} + F_{th} + \\ \frac{i\mathcal{D}_{\pm\vec{k}_{NU,i}}^{(Suhl)}}{2} \left(P_i\alpha_{\mp\vec{k}_{NU,i}}^* - P_i^*\alpha_{\mp\vec{k}_{NU,i}} \right) + \\ i\mathcal{D}_{\pm\vec{k}_{NU,i}}^{(SK)} \left(\alpha_{\pm\vec{k}_{NU,i}}^* \alpha_{\pm\vec{k}_{NU,i}} \alpha_{\pm\vec{k}_{NU,i}} - \right. \\ \left. \alpha_{\pm\vec{k}_{NU,i}} \alpha_{\pm\vec{k}_{NU,i}}^* \alpha_{\pm\vec{k}_{NU,i}}^* \right), \\ \\ \frac{dY_{\pm\vec{k}_{NU,i}}}{dt} &= (\omega'_{\pm\vec{k}_{NU,i}} + \omega_{\pm\vec{k}_{NU,i}})X_{\pm\vec{k}_{NU,i}} - \\ \alpha_G\omega_{\pm\vec{k}_{NU,i}}Y_{\pm\vec{k}_{NU,i}} + F'_{th} + \\ \frac{\mathcal{D}_{\pm\vec{k}_{NU,i}}^{(Suhl)}}{2} \left(P_i\alpha_{\mp\vec{k}_{NU,i}}^* + P_i^*\alpha_{\mp\vec{k}_{NU,i}} \right) + \\ \mathcal{D}_{\pm\vec{k}_{NU,i}}^{(SK)} \left(\alpha_{\pm\vec{k}_{NU,i}}^* \alpha_{\pm\vec{k}_{NU,i}} \alpha_{\pm\vec{k}_{NU,i}} + \right. \\ \left. \alpha_{\pm\vec{k}_{NU,i}} \alpha_{\pm\vec{k}_{NU,i}}^* \alpha_{\pm\vec{k}_{NU,i}}^* \right), \quad (33) \end{aligned}$$

where \vec{H}_A , \vec{H}_{dc} , \vec{H}_{th} are the anisotropy, applied dc, and white thermal noise magnetic fields, respectively. The Cartesian components \vec{H}_{th} are independent Gaussian fluctuators with variance $2\alpha_G k_B T / (\gamma M_s V)$. F_{th} and F'_{th} are independent Gaussian fluctuations with variance $2\alpha_G\omega_{\pm\vec{k}_{NU,i}}\bar{n}_{\pm\vec{k}_{NU,i}}$. To summarize, the nonlinear magnon interactions induce \vec{H}_{SW} in the LLG equation governing the macrospin dynamics \vec{m} , while the latter determines P_i that enters in finite- k magnon dynamics ($X_{\pm\vec{k}_{NU,i}}, Y_{\pm\vec{k}_{NU,i}}$), resulting in a closed EOM, that can be integrated numerically.

C. Results and discussion

1. Phenomenology

The stochastic switching frequency f_s is directly connected to the curvature of the free energy or force constant at each minimum. This manifests in the effective distribution function around the minima. When the minima and the saddle point of the macrospin free energy are

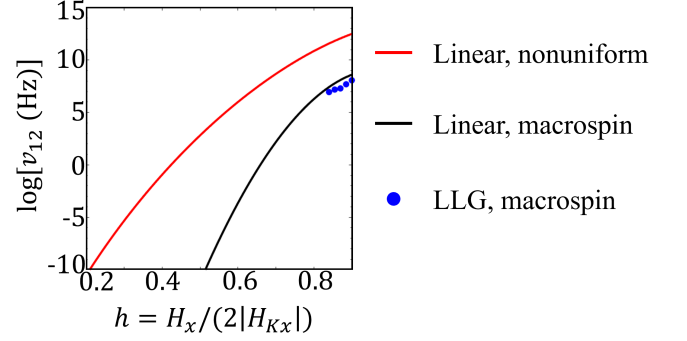


FIG. 4. Calculated transition frequency from the metastable to stable state, v_{12} , of an in-plane magnetization as a function of an external field H_x along the easy axis \hat{x} without taking into account the decay of the Kittel mode into spin waves. The easy axis in-plane anisotropy along \hat{x} , $H_{Kx} = -1.8$ T, the out-of-plane uniaxial hard axis anisotropy $H_{Kz}/H_{Kx} = -0.2$, $M_s = 3.8 \times 10^4$ A/m, $L = 150$ nm, $\mathcal{S} = \pi \times 5$ nm², $\mathcal{A}_{ex} = 5 \times 10^{-12}$ J/m, $\alpha_G = 0.01$, $\gamma = 28$ GHz/T. The black line is calculated from Brown's linear macrospin theory; red line is calculated from Braun's linear nonuniform theory; blue dots are numerically calculated from the macrospin LLG.

on the x axis, the Kittel mode occupation at each minimum

$$\langle m_x m_x \rangle = \frac{(u_0 + v_0)^2}{4} \{2\text{Re}\langle c_0 c_0 \rangle + 2\langle n_0 \rangle + 1\}, \quad (34)$$

while from EOM of ρ' (see Sec. II A),

$$\begin{aligned} \frac{d\langle c_{\vec{k}_{NU}} c_{-\vec{k}_{NU}} \rangle}{dt} &= i\Delta\omega_{\pm\vec{k}_{NU}} \langle c_{\vec{k}_{NU}} c_{-\vec{k}_{NU}} \rangle + \\ i2\mathcal{D}^{(Suhl)} \langle c_0 c_0 \rangle [2\langle n_{\pm\vec{k}_{NU}} \rangle + 1] &- 2\xi_{\pm\vec{k}_{NU}} \langle c_{\vec{k}_{NU}} c_{-\vec{k}_{NU}} \rangle, \quad (35) \end{aligned}$$

$$\begin{aligned} \frac{d\langle c_0 c_0 \rangle}{dt} &= i2\mathcal{D}^{(Suhl)} \langle c_{\vec{k}_{NU}} c_{-\vec{k}_{NU}} \rangle [2\langle n_0 \rangle + 1] - \\ 2\xi_0 \langle c_0 c_0 \rangle + \mathcal{F}, \quad (36) \end{aligned}$$

where we introduced the phenomenological \mathcal{F} as an effective force on $\langle c_0 c_0 \rangle$ that triggers the stochastic switching of \vec{m} . In Sec. II, we discussed the dependence of n_0 on the occupation of the \vec{k}_{NU} spin waves [see Eqs. (15)-(17)]. In the steady state

$$\begin{aligned} \text{Re}\langle c_0 c_0 \rangle &= \frac{\text{Re } \mathcal{F}}{2\xi_0 + \xi_{corr}}, \\ \xi_{corr} &= \frac{2\xi_{\pm\vec{k}_{NU}} (\mathcal{D}^{(Suhl)})^2 (2\langle n_0 \rangle + 1)(2\langle n_{\pm\vec{k}_{NU}} \rangle + 1)}{\Delta\omega_{\pm\vec{k}_{NU}}^2 + \xi_{\pm\vec{k}_{NU}}^2}. \quad (37) \end{aligned}$$

While it does not give a closed expression for f_s , Equation (37) tells us that at a fixed $\langle n_0 \rangle$ and $\langle n_{\pm\vec{k}_{NU}} \rangle$, the Suhl four magnon interaction $\mathcal{D}^{(Suhl)} \neq 0$, damps the correlation function $\text{Re}[\langle c_0 c_0 \rangle]$ by an additional ξ_{corr} , and

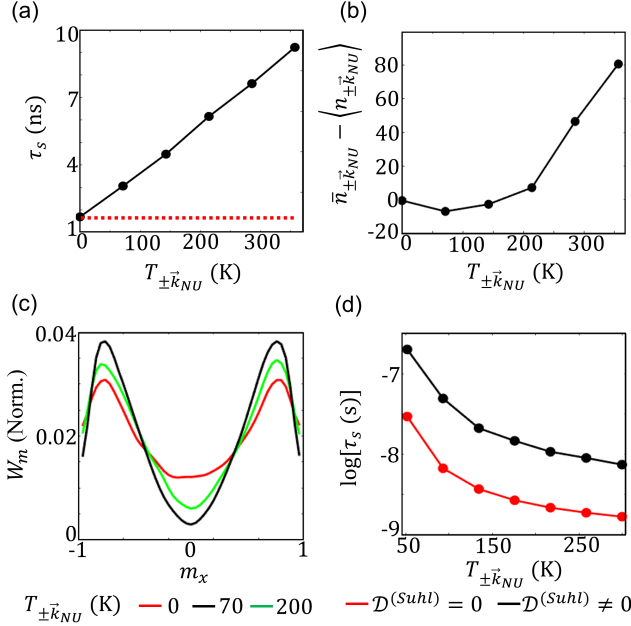


FIG. 5. (a) $\tau_s = 1/f_s$ as a function of the magnon temperature $T_{\vec{k}_{NU}}$. The red dashed line indicates τ_s when $\mathcal{D}^{(Suhl)} = 0$. (b) The dependence of $\bar{n}_{\vec{k}_{NU}} - \langle n_{\vec{k}_{NU}} \rangle$ on $T_{\vec{k}_{NU}}$. (c) The marginal distribution W_m of the magnetization along \hat{x} for different $T_{\vec{k}_{NU}}$. In (a)-(c), the macrospin environment temperature is fixed at $T_0 = 300$ K. (d) τ_s as a function of $T_0 = T_{\vec{k}_{NU}}$ without and with the Suhl nonlinear interaction, $\mathcal{D}^{(Suhl)} = 0$ (red) and $\mathcal{D}^{(Suhl)} \neq 0$ (black), respectively. The inset shows $\tau_r = \tau_s|_{\mathcal{D}^{(Suhl)} \neq 0} / \tau_s|_{\mathcal{D}^{(Suhl)} = 0}$. In (a)-(d), the sample diameter $r = 20$ nm, $\theta_s = \pi/4$, $H_{Kx} = -75$ mT, $H_{Kz} = 0.2$ T, and $M_s = 1.5 \times 10^6$ A/m.

thereby reduces $\langle m_x m_x \rangle$. In Sec. III C 2, we discuss the dependence of the numerically calculated f_s in terms of the brake on the dynamics caused by ξ_{corr} .

2. Numerical results and discussion

Here we first report numerical micromagnetic results without spin waves and compare them with Brown's and Braun's theories, then turning to calculations for our spin wave model.

With Fig. (4) we report that v_{12} from a numerical solution of the LLG calculation for the macrospin $v_{12}^{(MS,LLG)}$ is only slightly lower than the model $v_{12}^{(Brown)}$, justifying Kramers escape model.

Next, we discuss the stochastic LLG equation for the domain wall assisted switching based on the Braun theory. We focus here on the experimentally most interesting in-plane magnetized samples with $H_{Kx} = \mu_0 M_s K_x = -1.8$ T and a relatively weak out-of-plane hard uniaxial anisotropy, $H_{Kz}/H_{Kx} = -0.2$. A magnetic field H_x applied in the \hat{x} direction shifts the two energy minima with respect to each other and v_{12} is the transi-

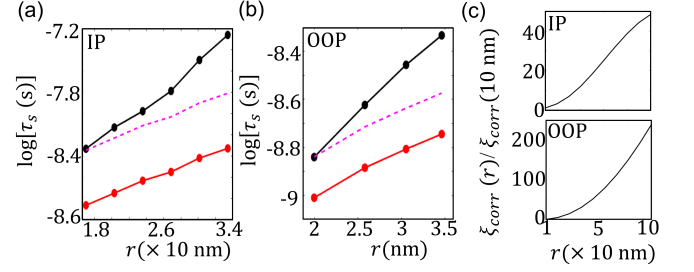


FIG. 6. Sample radius dependence. (a)-(b) τ_s as a function of r when $\mathcal{D}^{(Suhl)} = 0$ (red dots) and $\mathcal{D}^{(Suhl)} \neq 0$ (black dots). The magenta dashed lines are shifted red lines for scale comparison with the black lines. (a) and (b) correspond to the IP and OOP cases, respectively. $T_0 = T_{\vec{k}_{NU}}$ in (a) and (b). In (b), $H_{Kx} = -50$ mT. (c)-(d) ξ_{corr} as a function of r . (c) and (d) correspond to the IP and OOP cases, respectively.

tion from the high to the low state. We may then plug $E(\theta_1) = -H_x M_s$, $E(\theta_{sd}) = H_{Kx} M_s (1 + \epsilon^2)$, $\lambda_{sd,\phi} = -2H_{Kx} M_s (\epsilon^2 - 1)$, $\lambda_{sd,\theta} = 2H_{Kz} M_s (1 - \epsilon^2)$, $\lambda_{1,\phi} = -2H_{Kx} M_s + 2H_{Kz} M_s + H_x M_s$, $\lambda_{1,\theta} = -2H_{Kx} M_s + H_x M_s$, and $\epsilon = H_x / (2H_{Kx})$ into the Braun theory Eq. (23). We use the Braun formula simplified from Eq. (25) [35], viz.

$$v_{12} \approx 2\gamma |H_{Kx}| \Omega \exp^{-2S\sqrt{A_{ex}|H_{Kx}|M_s}\mathcal{E}}, \quad (38)$$

where

$$\Omega = 16\pi^{-3/2} \alpha_G L \sqrt{2\beta S \sqrt{A_{ex}|H_{Kx}|M_s} [\sqrt{Q} + \sqrt{1+Q}]^2} \exp[-R] \quad (39)$$

$\mathcal{E} = 4 \tanh R - 4R \operatorname{sech}^2 R$, $R = \operatorname{sech}^{-1} \sqrt{h}$, $h = H_x / (2|H_{Kx}|)$, and $Q = H_{Kz} / |H_{Kx}|$.

Figure 4 shows that v_{12} as calculated by Braun's theory $v_{12}^{(Braun)}$ is significantly larger than estimated by the macrospin result $v_{12}^{(Brown)}$ because the saddle point of the free energy is significantly lowered by domain walls. On the other hand, we found only weak non-linear effects on the ratios v_{12}/v_{21} (not shown).

Now we are ready to discuss the effect of spin waves with finite wave vector and their interaction with the macrospin, based on our three-mode model of Sec. III B. We compute spin wave frequencies (i.e. detuning $\Delta\omega_{\pm\vec{k}_{NU}}$) and coefficients $\mathcal{D}^{(Suhl)}$, $\mathcal{D}_{\vec{k}}^{(SK)}$, and $\mathcal{D}^{(CK)}$ for the ultrathin films with $d = 2$ nm [45] used in the MTJ experiments [4, 22, 42, 43]. The dispersion of coefficients and frequencies are evaluated for the lowest frequency in-plane standing waves with $\vec{k}_{NU,+(-)} = (\pi/r)\vec{m}_{1(2)}$ [see Fig. 1(a)], where r is the radius of the sample. For the IP magnetized sample, at a certain $|\vec{k}|$, $\omega_{\vec{k}}$ and interaction coefficients are functions of the in-plane angle between the magnetization and \vec{k} , $\theta_{\vec{k}}$. The detuning $\Delta\omega_{\pm\vec{k}_{NU}}$ and interaction coefficients are smallest and strongest, respectively, for $\theta_{\vec{k}} = 0$. Therefore, for the IP configuration, we choose $\vec{k}_{NU,+(-)}$ with $\theta_{\vec{k}_{NU,+(-)}} = 0$. For the OOP

magnetized sample, $\omega_{\vec{k}}$ and interaction coefficients are isotropic for in-plane \vec{k} , so the choice of in-plane angle for $\vec{k}_{NU,+(-)}$ does not matter. In the elliptical samples of Ref. [42], an IP easy axis leads to a θ_s -dependence of $|\vec{k}_{NU}|$ with changing θ_s that we disregard here. Therefore, for the IP magnetized sample

$$\begin{aligned}\Delta\omega_{\pm\vec{k}_{NU}} &\approx \omega_M \sqrt{|H_{Ke}H_{Kh}|} \frac{A_{ex}k_{NU}^2}{2|H_{Ke}\cos\theta_s|}, \\ \mathcal{D}^{(Suhl)} &\approx \frac{\omega_M}{2} \{ [H_{Kh} + A_{ex}k_{NU}^2 + H_{Ke} \times \\ &(\sin^2\theta_s - 2\cos^2\theta_s)] u_0^2 + \\ &[3(H_{Ke}\sin^2\theta_s - H_{Kh})] u_0 v_0 \}, \\ u_0 &\approx \sqrt{\frac{1}{4} \sqrt{\frac{H_{Kh}}{|H_{Ke}|\cos^2\theta_s} + \frac{1}{2}}}, \\ v_0 &\approx \sqrt{\frac{1}{4} \sqrt{\frac{H_{Kh}}{|H_{Ke}|\cos^2\theta_s} - \frac{1}{2}}}.\end{aligned}\quad (40)$$

For the OOP samples,

$$\begin{aligned}\Delta\omega_{\pm\vec{k}_{NU}} &\approx \omega_M |H_{Ke}| A_{ex} k_{NU}^2, \\ \mathcal{D}^{(Suhl)} &\approx \frac{\omega_M}{2} \times (-2|H_{Ke}| + 2A_{ex}k_{NU}^2) u_0^2, \\ u_0 &= 1, v_0 = 0.\end{aligned}\quad (41)$$

In the following we focus on the IP case, but the main conclusions hold for the OOP samples. First, we explore the dependence of $\tau_s = 1/f_s$ on the spin-wave temperature $T_{\pm\vec{k}_{NU},i} = T_{\pm\vec{k}_{NU}}$ for constant macrospin reservoir temperature $T_0 = 300$ K constant at . According to Figure 5(a) τ_s monotonically increases with $T_{\pm\vec{k}_{NU}}$ as expected since $\xi_{corr} \propto \langle n_{\pm\vec{k}_{NU}} \rangle \propto T_{\pm\vec{k}_{NU}}$. When $T_{\pm\vec{k}_{NU}} \rightarrow 0$ there are no \vec{k}_{NU} magnons and $\xi_{corr} \rightarrow 0$, i.e. τ_s becomes that when $\mathcal{D}^{(Suhl)} \rightarrow 0$ [see the red dotted line in Fig. 5(a)]. Figure 5(b) shows that $\bar{n}_{\pm\vec{k}_{NU}} - \langle n_{\pm\vec{k}_{NU}} \rangle < 0$ for small $T_{\pm\vec{k}_{NU}}$, and becomes positive with increasing $T_{\pm\vec{k}_{NU}}$. This is in line with our analysis in Sec. II of the balance between the effective temperatures of the Kittel mode and magnon pair [see Fig. 1(c) bottom panel]. The probability distribution W_{m_x} of the magnetization along the \hat{x} direction in Figure 5(c) shows an increasing localization at the energy minima with increasing $T_{\pm\vec{k}_{NU}}$, reflecting the increased damping of the fluctuations expected from Sec. III C 1.

Next, we study the dependence on $T_0 = T_{\pm\vec{k}_{NU}} = T$. According to Figure 4(d) τ_s is always enhanced when the Suhl interaction $\mathcal{D}^{(Suhl)} \neq 0$. The ratio

$$\tau_r = \frac{\tau_s|_{\mathcal{D}^{(Suhl)} \neq 0}}{\tau_s|_{\mathcal{D}^{(Suhl)} = 0}} \gg 1 \quad (42)$$

does not depend strongly on T which proves that spin waves mainly affect the attempt frequency τ_0 , in agreement with experiments [42]. In the experiments by Kanai

et al. [42], we extract τ_0 by measuring f_s from resistance fluctuations in tunneling magneto-resistance, as a function of θ_s . The latter is varied by changing the magnetic field along \hat{y} [see Fig. 3(a), top panel], leading to τ_0 estimations an order of magnitude larger than what is expected from macrospin LLG calculations or Brown theory.

From an application point of view it is of great interest to reduce the switching time by changing the sample dimensions [30]. Figures 6(a) and (b) show that τ_r indeed decreases with the sample radius r for both the IP and OOP samples. ξ_{corr} [see Eq. (37)] in Fig. 6(c) monotonically increases with r , since $\Delta\omega_{\pm\vec{k}_{NU}} \gg \xi_{\pm\vec{k}_{NU}}$, $\Delta\omega_{\pm\vec{k}_{NU}} \propto 1/r^2$, and $\xi_{\pm\vec{k}_{NU}} = \alpha_G \omega_{\pm\vec{k}_{NU}} \propto (a + b/r^2)$, $\langle n_{\pm\vec{k}_{NU}} \rangle \propto 1/\omega_{\pm\vec{k}_{NU}}$, and $\mathcal{D}^{(Suhl)} \propto (a' + b'^2)$, where a , a' , b and b' are constants related to material parameters [see Eqs. (40)-(41)]. This dependence agrees with recent observations [43] of an increase of τ_0 with r for OOP samples in contrast to the Néel-Brown theory that predicts a decrease in τ_0 with magnetic volume [see Eq. (22)].

IV. CONCLUSION

We theoretically study the interactions of uniform magnetization precession with finite-momentum spin waves at finite temperatures on fluctuations around the equilibrium magnetizations and the stochastic switching dynamics of the magnetization between two equilibrium directions. We analytically and numerically show that a four-magnon interaction attracts magnon numbers of the Kittel mode and coupled spin waves, while suppressing the random switching of the magnetization. The temperature affects the stochastic switching frequency dominantly via the attempt frequency that decreases with the effective temperature of the interacting finite- k spin waves. Shrinking the sample for a fixed film thickness increases the attempt frequency. The performance of MTJs in applications such as probabilistic computing can therefore be boosted by shrinking the sample dimensions and selective cooling of spin waves with finite momenta. Future theories and experiments should be designed to explore the active cooling. Theoretically, more in-depth analytical and numerical models should delineate the intricacies of nonlinear interactions as well as domain wall nucleation and motion that may cause numerical corrections to switching frequencies computed here.

ACKNOWLEDGMENTS

We acknowledge support by JSPS KAKENHI (Grants Nos. 21K13847, 19H00645, 22H04965, 20H02178, 24H02231, 24H02235, 24H00039), JST CREST (Grant No. JPMJCR19K3), JST-ASPIRE (Grant No. JPM-JAP2322), JST PRESTO (Grant No. JPMJPR21B2), MEXT X-NICS JPJ011438, Shimadzu Science Founda-

tion, Takano Research Foundation, and Cooperative Research Projects of RIEC.

-
- [1] L. Néel, *Theorie du trainage magnetique des ferromagnetiques en grains fins avec application aux terres cuites*, Ann. Geophys. **5**, 99 (1949).
- [2] W. F. Brown, *Thermal Fluctuations of a Single-Domain Particle*, Phys. Rev. **130**, 1677 (1963).
- [3] W. F. Brown, *Thermal Fluctuations of Fine Ferromagnetic Particles*, IEEE Trans. Mag. **15**, 1196 (1979).
- [4] K. Hayakawa, S. Kanai, T. Funatsu, J. Igarashi, B. Jinnai, W. A. Borders, H. Ohno, and S. Fukami, *Nanosecond Random Telegraph Noise in In-Plane Magnetic Tunnel Junctions*, Phys. Rev. Lett. **126**, 117202 (2021).
- [5] C. Safranski, J. Kaiser, P. Trouilloud, P. Hashemi, G. Hu, and J. Z. Sun, *Demonstration of Nanosecond Operation in Stochastic Magnetic Tunnel Junctions*, Nano. Lett. **21**, 2040-2045 (2021).
- [6] E. M. Chudnovsky and L. Gunther, *Quantum Tunneling of Magnetization in Small Ferromagnetic Particles*, Phys. Rev. Lett. **60**, 661 (1988).
- [7] D. D. Awschalom, J. F. Smyth, G. Grinstein, D. P. DiVincenzo, and D. Loss, *Macroscopic Quantum Tunneling in Magnetic Proteins*, Phys. Rev. Lett. **68**, 3092 (1992).
- [8] H. Barkhausen, Phys. Z. **20**, 401 (1919).
- [9] Djordje Spasojevic, Srdjan Bukvic, Sava Milosevic, and H. Eugene Stanley, *Barkhausen noise: Elementary signals, power laws, and scaling relations*, Phys. Rev. E **54**, 2531 (1996).
- [10] D. Lachance-Quirion, S. P. Wolski, Y. Tabuchi, S. Kono, K. Usami, and Y. Nakamura, *Entanglement-based single-shot detection of a single magnon with a superconducting qubit*, Science **367**, 425 (2020).
- [11] M. Elyasi, Y. M. Blanter, G. E. W. Bauer, *Resources of nonlinear cavity magnonics for quantum information*, Phys. Rev. B **101**, 054402 (2020).
- [12] H. Yuan, Y. Cao, A. Kamra, R. A. Duine, and P. Yan, *Quantum magnonics: When magnon spintronics meets quantum information science*, Phys. Rep. **965**, 1 (2022).
- [13] B. Z. Rameshti, S. V. Kusminskiy, J. A. Haigh, K. Usami, D. Lachance-Quirion, Y. Nakamura, C.-M. Hu, H. X. Tang, G. E. W. Bauer, and Y. M. Blanter, *Cavity magnonics*, Phys. Rep. **979**, 1 (2022).
- [14] A. Chumak et al., *Advances in magnetics roadmap on spin-wave computing*, IEEE Trans. Magn. **58**, 1 (2022).
- [15] T. Hioki, H. Shimizu, T. Makiuchi, and E. Saitoh, *State tomography for magnetization dynamics*, Phys. Rev. B **104**, L100419 (2021).
- [16] T. Makiuchi, T. Hioki, H. Shimizu, K. Hoshi, M. Elyasi, K. Yamamoto, N. Yokoi, A. Serga, B. Hillebrands, G. E. W. Bauer, and E. Saitoh, *Persistent magnetic coherence in magnets*, Nat. Mater. (2024).
- [17] T. Makiuchi, T. Hioki, Y. Shimazu, Y. Oikawa, N. Yokoi, S. Daimon, and E. Saitoh, *Parametron on magnetic dot: Stable and stochastic operation*, Appl. Phys. Lett. **118**, 022402 (2021).
- [18] M. Elyasi, E. Saitoh, and G. E. W. Bauer, *Stochasticity of the magnon parametron*, Phys. Rev. B **105**, 054403 (2022).
- [19] D. E. Endean, C. T. Weigelt, R. H. Victora, and E. Dan Dahlberg, *Tunable random telegraph noise in individual square permalloy dots*, Appl. Phys. Lett. **104**, 252408 (2014).
- [20] P. Talatchian, M. W. Daniels, A. Madhavan, M. R. Puffall, E. Jue, W. H. Rippard, J. J. McClelland, and M. D. Stiles, *Mutual control of stochastic switching for two electrically coupled superparamagnetic tunnel junctions*, Phys. Rev. B **104**, 054427 (2021).
- [21] K. Y. Camsari, R. Faria, B. M. Sutton, and S. Datta, *Stochastic p-Bits for Invertible Logic*, Phys. Rev. X **7**, 031014 (2017).
- [22] W. A. Borders, A. Z. Pervaiz, S. Fukami, K. Y. Camsari, H. Ohno, and S. Datta, *Integer factorization using stochastic magnetic tunnel junctions*, Nature **573**, 390-393 (2019).
- [23] D. Vodenicarevic, N. Locatelli, A. Mizrahi, J. S. Friedman, A. F. Vincent, M. Romera, A. Fukushima, K. Yakushiji, H. Kubota, S. Yuasa, S. Tiwari, J. Grollier, and D. Querlioz, *Low-Energy Truly Random Number Generation with Superparamagnetic Tunnel Junctions for Unconventional Computing*, Phys. Rev. Appl. **8**, 54045 (2017).
- [24] A. Mizrahi, T. Hirtzlin, A. Fukushima, H. Kubota, S. Yuasa, J. Grollier, and D. Querlioz, *Neural-like computing with populations of superparamagnetic basis functions*, Nat. Commun. **9**, 1533 (2018).
- [25] J. Kaiser, W. A. Borders, K. Y. Camsari, S. Fukami, H. Ohno, and S. Datta, *Hardware-Aware In Situ Learning Based on Stochastic Magnetic Tunnel Junctions*, Phys. Rev. Appl. **17**, 014016 (2022).
- [26] N. S. Singh, K. Kobayashi, Q. Cao, K. Selcuk, T. Hu, S. Niazi, N. A. Aadit, S. Kanai, H. Ohno, S. Fukami, K. Y. Camsari, *CMOS plus stochastic nanomagnets enabling heterogeneous computers for probabilistic inference and learning*, Nat. Commun. **15**, 2685 (2024).
- [27] J. Si, S. Yang, Y. Cen, J. Chen, Y. Huang, Z. Yao, D.-J. Kim, K. Cai, J. Yoo, X. Fong, H. Yang, *Energy-efficient superparamagnetic Ising machine and its application to traveling salesman problems*, Nat. Commun. **15**, 3457 (2024).
- [28] S. Ikeda, K. Miura, H. Yamamoto, K. Mizunuma, H. D. Gan, M. Endo, S. Kanai, J. Hayakawa, F. Matsukura, H. Ohno, *A perpendicular-anisotropy CoFeB-MgO magnetic tunnel junction*, Nat Mater **9**, 721 (2010).
- [29] K. Watanabe, B. Jinnai, S. Fukami, H. Sato, and H. Ohno, *Shape anisotropy revisited in single-digit nanometer magnetic tunnel junctions*, Nat. Commun. **9**, 663 (2018).
- [30] B. Jinnai, K. Watanabe, S. Fukami, and H. Ohno, *Scaling magnetic tunnel junction down to single-digit nanometers-Challenges and prospects*, Appl. Phys. Lett. **116**, 160501 (2020).
- [31] T. Funatsu, S. Kanai, J. Ieda, S. Fukami, and H. Ohno, *Local bifurcation with spin-transfer torque in superparamagnetic tunnel junctions*, Nat. Commun. **13**, 4079 (2022).
- [32] H. A. Kramers, *Brownian motion in a field of force and the diffusion model of chemical reactions*, Physica **7**, 284 (1940).

- [33] H.-B. Braun, *Thermally Activated Magnetization Reversal in Elongated Ferromagnetic Particles*, Phys. Rev. Lett. **71**, 3557 (1993).
- [34] H.-B. Braun, *Kramers rate theory, broken symmetries, and magnetization reversal (invited)*, J. Appl. Phys. **76**, 6310 (1994).
- [35] H.-B. Braun, *Statistical mechanics of nonuniform magnetization reversal*, Phys. Rev. B **50**, 16501 (1994).
- [36] H.-B. Braun, *Fluctuations and instabilities of ferromagnetic domain-wall pairs in an external magnetic field*, Phys. Rev. B **50**, 16485 (1994).
- [37] S. Krause, G. Herzog, T. Stapelfeldt, L. Berbil-Bautista, M. Bode, E.Y. Vedmedenko, and R. Wiesendanger, *Magnetization Reversal of Nanoscale Islands: How Size and Shape Affect the Arrhenius Prefactor*, Phys. Rev. Lett. **103**, 127202 (2009).
- [38] P. F. Bessarab, V. M. Uzdin, and H. Jonsson, *Size and Shape Dependence of Thermal Spin Transitions in Nanoislands*, Phys. Rev. Lett. **110**, 020604 (2013).
- [39] G. Sala, J. Meyer, A. Flechsig, L. Gabriel, and P. Gambardella, *Deterministic and stochastic aspects of current-induced magnetization reversal in perpendicular nanomagnets*, Phys. Rev. B **107**, 214447 (2023).
- [40] S. Kanai, K. Hayakawa, H. Ohno, and S. Fukami, *Theory of relaxation time of stochastic nanomagnets*, Phys. Rev. B **103**, 094423 (2021).
- [41] S. Arrhenius, *Über die Reaktionsgeschwindigkeit bei der Inversion von Rohrzucker durch Säuren*, Zeitschrift für Physikalische Chemie. **4U**, 226 (1889).
- [42] S. Kanai, K. Hayakawa, M. Elyasi, K. Kobayashi, J. Igarashi, B. Jinnai, W. A. Borders, G. E. W. Bauer, H. Ohno, and S. Fukami, *Stochastic switching time constant and instability in nanomagnets*, submitted.
- [43] H. Kaneko, R. Ota, K. Kobayashi, S. Kanai, M. Elyasi, G. E. W. Bauer, H. Ohno, and S. Fukami, *Temperature dependence of the properties of stochastic magnetic tunnel junction with perpendicular magnetization*, APEX **17**, 053001 (2024).
- [44] M. Aspelmeyer, T. J. Kippenberg, and F. Marquardt, *Cavity optomechanics*, Rev. Mod. Phys. **86**, 1391 (2014).
- [45] P. Krivosik and C. E. Patton, *Hamiltonian formulation of nonlinear spin-wave dynamics: Theory and applications*, Phys. Rev. B **82**, 184428 (2010).
- [46] H. J. Carmichael, *Statistical Methods in Quantum Optics 1*, Springer (1999).
- [47] D. F. Walls and G. J. Milburn, *Quantum Optics*, Springer (2008).
- [48] H. Suhl, *The Theory of Ferromagnetic Resonance at High Signal Powers*, Phys. Chem. Solids **1**, 209 (1957).
- [49] V. S. Lvov, *Wave Turbulence Under Parametric Excitation*, (Springer-Verlag, 1994).
- [50] S. M. Rezende, *Fundamentals of magnonics*, Springer, Berlin, (2020).
- [51] H. Kurebayashi, O. Dzyapko, V. E. Demidov, D. Fang, A. J. Ferguson, and S. O. Demokritov, *Controlled enhancement of spin-current emission by three-magnon splitting*, Nat. Mater. **10**, 660 (2011).
- [52] O. Lee, K. Yamamoto, M. Umeda, C. W. Zollitsch, M. Elyasi, T. Kikkawa, E. Saitoh, G. E. W. Bauer, H. Kurebayashi, *Nonlinear magnon polaritons*, Phys. Rev. Lett. **130**, 046703 (2023).
- [53] L. Sheng, M. Elyasi, J. Chen, W. He, Y. Wang, H. Wang, H. Feng, Y. Zhang, I. Medlej, S. Liu, W. Jiang, X. Han, D. Yu, J.-P. Ansermet, G. E. W. Bauer, H. Yu, *Nonlocal Detection of Interlayer Three-Magnon Coupling*, Phys. Rev. Lett. **130**, 046701 (2023).
- [54] H. J. Carmichael, *Statistical Methods in Quantum Optics 2*, Springer (2008).
- [55] J.-S. Langer, *Statistical Theory of the Decay of Metastable States*, Ann. Phys. **54**, 258 (1969).
- [56] R. Landauer and J. A. Swanson, *Frequency Factors in the Thermally Activated Process*, Phys. Rev. **121**, 1668 (1961).
- [57] P. Kinsler and P. D. Drummond, *Quantum dynamics of the parametric oscillator*, Phys. Rev. A **43**, 6194 (1991).